



A Journal of the Gesellschaft Deutscher Chemiker

# Angewandte Chemie

GDCh

International Edition

www.angewandte.org

## Accepted Article

**Title:** NIR-II Chemiluminescence Molecular Sensor for In-Vivo High Contrast Inflammation Imaging

**Authors:** Fan Zhang, Yanling Yang, Shangfeng Wang, Lingfei Lu, Qisong Zhang, Peng Yu, and Yong Fan

This manuscript has been accepted after peer review and appears as an Accepted Article online prior to editing, proofing, and formal publication of the final Version of Record (VoR). This work is currently citable by using the Digital Object Identifier (DOI) given below. The VoR will be published online in Early View as soon as possible and may be different to this Accepted Article as a result of editing. Readers should obtain the VoR from the journal website shown below when it is published to ensure accuracy of information. The authors are responsible for the content of this Accepted Article.

**To be cited as:** *Angew. Chem. Int. Ed.* 10.1002/anie.202007649

**Link to VoR:** <https://doi.org/10.1002/anie.202007649>

## COMMUNICATION

# NIR-II Chemiluminescence Molecular Sensor for *In-Vivo* High Contrast Inflammation Imaging

Yanling Yang, Shangfeng Wang, Lingfei Lu, Qisong Zhang, Peng Yu, Yong Fan\* and Fan Zhang\*

**Abstract:** Chemiluminescence (CL) sensing without the external excitation light and autofluorescence interference has been applied to high-contrast *in vitro* immunoassays and *in vivo* inflammation and tumor microenvironment detection. However, conventional CL sensing usually operates in the range of 400–850 nm, which limits the high-performance of *in vivo* imaging due to the serious light scattering effect and signals attenuation in tissue. To address this challenge, here we present a new type of CL sensor in the second near-infrared window (NIR-II CLS) with deep penetration depth (~ 8 mm) by employing successive CL resonance energy transfer (CRET) and Förster resonance energy transfer (FRET) from the activated CL substrate to two rationally designed donor-acceptor-donor fluorophores BTD540 and BBTD700. NIR-II CLS can be selectively activated by hydrogen peroxide over other reactive oxygen species (ROSs). Moreover, NIR-II CLS is capable of detecting local inflammation in mice with 4.5-fold higher signal-to-noise ratio (SNR) than that under NIR-II fluorescence modality.

Optical sensing has become a vital technique for noninvasive and real-time visualization of biological events with superior spatio-temporal resolution.<sup>[1]</sup> Fluorescence (FL) is a common modality for optical sensing that requires an excitation light source to light up the fluorescent reporters. In recent years, researchers took advantages of reduced photon scattering, and barely existed tissue autofluorescence background in the second near-infrared window (NIR-II, 1000–1700 nm) to develop various fluorescent probes for *in vivo* NIR-II imaging.<sup>[2]</sup> Even though, the external excitation light can still cause autofluorescence background from endogenous biomolecules in FL sensing and imaging.<sup>[3]</sup> Moreover, the major light absorbers like hemoglobins and water in biological tissue can turn excitation photons into heat dissipation,<sup>[4]</sup> which also hampers the long-time observation. In contrast, chemiluminescence (CL) could conquer these limitations because it eliminates the demand of excitation light source.<sup>[5]</sup> Classical peroxyoxalate-based CL (POCL) is a nonradiative dipole-dipole energy transfer process<sup>[6,7]</sup> from a CL donor (1,2-dioxetanedione intermediate, DOD) to a suitable acceptor by the chemical reaction between hydrogen peroxide (H<sub>2</sub>O<sub>2</sub>) and peroxyoxalate, which involved a chemically initiated electron exchange luminescence mechanism.<sup>[8]</sup> POCL systems commonly emit in the visible region, and it is readily absorbed and scattered by the molecules and cells in biological matrices<sup>[9]</sup>. Currently, the CL wavelengths have been successfully extended to red light to improve the potential bioapplication by CRET between activated

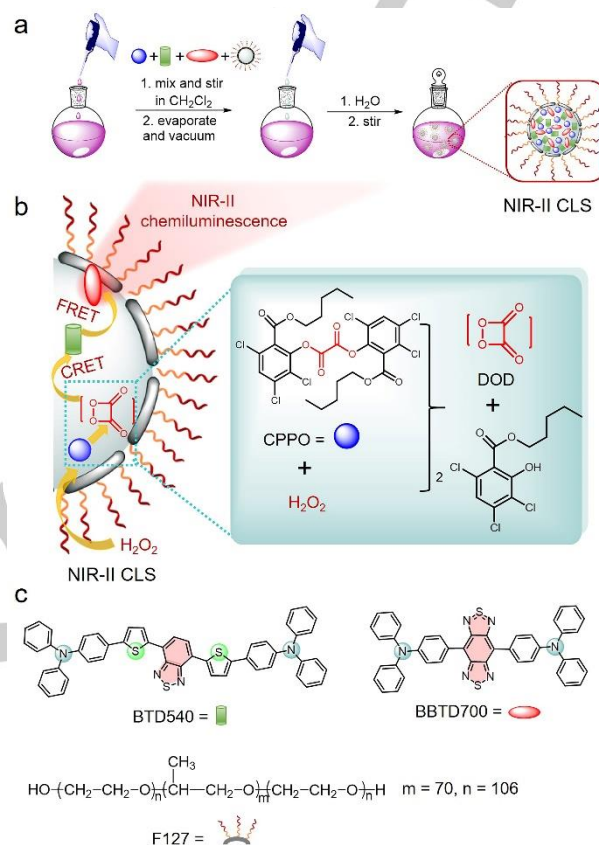


**Figure 1.** (a) The preparation scheme of NIR-II CLS. (b) The illustration of the principle for generating NIR-II CL emission in the presence of H<sub>2</sub>O<sub>2</sub>. (c) The structure of BTD540, BBTD700 and F127.

CL substrates and other fluorescent dyes,<sup>[10–13]</sup> or to increase the conjugation of the Schaap's adamantylidene-dioxetane system<sup>[14]</sup>. Due to external light-free luminescence, POCL has been widely used for high-contrast immunoassays<sup>[15]</sup> and tumor microenvironment<sup>[9,10]</sup> detection. However, the penetration depth and SNR for *in vivo* CL imaging in the reported wavelength region remain to be improved. Developing CL in the NIR-II region is promising to address this issue, which however remains a great challenge.

Herein, we report the NIR-II CL sensor (NIR-II CLS) for high contrast *in vivo* inflammation imaging based on a classical POCL system. In our design, two donor-acceptor-donor (D-A-D) fluorescent dyes (BTD540 and BBTD700) are used to transduce the high energy of CL donor (DOD) to NIR-II photons by integrating successive CRET (DOD-to-BTD540) and FRET (BTD540-to-BBTD700) processes (Figure 1). The large Stokes shift (> 100 nm) of both BTD540 and BBTD700 and the extremely high FRET efficiency (94.12%) between them play crucial roles for the efficient NIR-II CL. Furthermore, NIR-II CLS can be selectively activated by H<sub>2</sub>O<sub>2</sub> over other reactive oxygen species

Y. Yang, S. Wang, L. Lu, Q. Zhang, P. Yu, Prof. Y. Fan, and Prof. F. Zhang  
 Department of Chemistry, State Key Laboratory of Molecular Engineering of Polymers and iChem, Shanghai Key Laboratory of Molecular Catalysis and Innovative Materials  
 Fudan University  
 Shanghai 200433, China.  
 E-mail: [fan\\_yong@fudan.edu.cn](mailto:fan_yong@fudan.edu.cn), [zhang\\_fan@fudan.edu.cn](mailto:zhang_fan@fudan.edu.cn)  
 Supporting information for this article is given via a link at the end of the document.

## COMMUNICATION

(ROs) under physiological conditions with long duration (60 min) and deeper penetration depth ( $\sim 8$  mm), allowing for *in vivo* detection of the  $H_2O_2$ -induced local inflammation in lymph node and arthritis region of the mice. Compared with NIR-II FL sensing in the same system, 4.5-fold enhancement in SNR was achieved for NIR-II CL sensing, showing a great promise for *in vivo* biosensing.

The synthesis procedure of NIR-II CLS is shown in the Figure 1a. The CL substrate bis[3,4,6-trichloro-2-(pentylloxycarbonyl)phenyl]oxalate (CPPO) is oxidized by  $H_2O_2$  to generate the unstable 1,2-dioxetanedione (DOD) intermediate, which then transfers chemical energy to BTD540 through CRET process, and subsequently to BBTD700 through FRET to provide CL signals in the NIR-II region (Figure 1b). BTD540 and BBTD700 were synthesized by simple one-step Suzuki coupling reaction under a nitrogen atmosphere (Scheme S4 and S5) with the absorption/emission peaks at 540/680 nm and 700/985 nm (Figure S1a and S1b, Figure S2a and S2b), respectively. The Stokes shift of BTD540 and BBTD700 are up to 140 and 285 nm, respectively. The two dyes compose a potentially efficient FRET pair due to the large spectral overlapping integrals (Figure 2a).

To verify our design for the NIR-II CL molecular sensor, we first incorporated the CPPO, BTD540 (CRET acceptor) into polymeric surfactant F127 (termed as BTD540 micelle) to validate the CRET process. The optimal conditions were screened by tuning the amount of BTD540, which were obtained at 1.6% (Figure S3). Under this circumstance, BTD540 micelle showed the average diameter and hydrodynamic size of  $21 \pm 2.6$  nm (TEM, Figure S4b) and  $\sim 18$  nm (DLS, Figure S4a), respectively. Compared with BTD540 solution dissolved in  $CH_2Cl_2$ , BTD540 micelle dispersed in  $H_2O$  showed similar absorption spectra (Figure S1a), and the slight blue-shift of the FL signal was due to the self-aggregation of BTD540 (Figure S1b). Upon the addition of  $H_2O_2$  to BTD540 micelle, an apparent CL signal was observed with emission peak shape similar to the FL signal (Figure 2b), indicating the successful occurrence of CRET process.

We then incorporated the BTD540 and BBTD700 into polymeric surfactant F127 to further verify the efficiency of the secondary FRET process. By increasing BBTD700/BTD540 mole ratio from 0:1 to 10:1 in micelle, the FL intensity ratio of BBTD700 to BTD540 was increased by 16-fold under 540 nm excitation, suggesting that efficient FRET process occurred between BTD540 and BBTD700 (Figure 2c). The highest FRET efficiency between BTD540 and BBTD700 was determined to be 94.12% with the BBTD700/BTD540 mole ratio of 5:1<sup>[16]</sup>. The Förster distances ( $R_0$ ) of these two dyes were also calculated to be 1.6 nm, which guarantee the efficient FRET between the dyes and bridge the chemical energy to the NIR-II region (see supplementary information).

Based on the above analysis, we prepared the biocompatible NIR-II CLS by incorporating optimal amount of BTD540, BBTD700 and CPPO molecules into the hydrophobic interior of F127 micelles (Table S1). The diameter and the hydrodynamic size of the as-prepared NIR-II CLS are  $23 \pm 3.0$  nm (TEM, Figure 2d) and  $\sim 21$  nm (DLS, Figure 2d insert), respectively. In the NIR-II CLS, the absorbance of BTD540 ( $\lambda_{abs, max} = 540$  nm) and BBTD700 ( $\lambda_{abs, max} = 700$  nm) were simultaneously observed (Figure S2a). Compared to the BBTD700 molecule in  $CH_2Cl_2$ , the

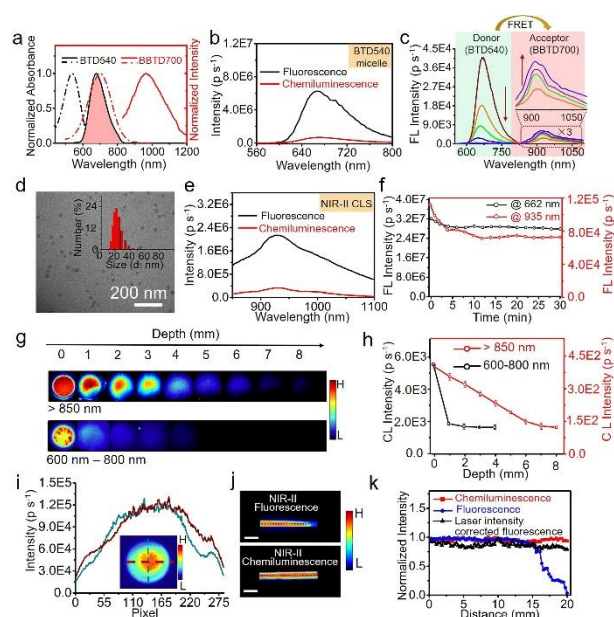


**Figure 2.** (a) Normalized absorbance (dash dot line) and emission (solid line) spectra of BTD540 (black line) and BBTD700 (red line) in  $CH_2Cl_2$ . (b) FL (black curve,  $\lambda_{ex} = 540$  nm) and CL spectra (red curve) of micelles containing only BTD540. (c) Emission spectra of BTD540 and BBTD700 mixtures in  $CH_2Cl_2$  ( $\lambda_{ex} = 540$  nm). The molar ratio of BBTD700/BTD540 is 0 (dark red curve), 1:1 (orange curve), 2:1 (green curve), 5:1 (blue curve), 10:1 (purple curve), respectively. (d) TEM image of NIR-II CLS. Insert: DLS of NIR-II CLS. (e) FL (black curve,  $\lambda_{ex} = 540$  nm) and CL (red curve) spectra of NIR-II CLS in the presence of  $H_2O_2$  (19 mM). (f) Time-course of fluorescence intensities of micelles containing only BTD540 and BBTD700 with emissions at 662 nm and 935 nm in the presence of  $H_2O_2$  (19 mM) under 540 nm and 700 nm excitation, respectively. (g) CL signals of NIR-II CLS in 96-well plate through stacked slices of chicken ham at varied depth in different detection windows. (h) Corresponding CL intensity of NIR-II CLS with stacked slices of chicken ham in (g). (i) Intensity profiles along the dashed lines with the same color in a (insert) Gaussian point spread function facula. (j) Optical images of capillaries filled with NIR-II CLS for NIR-II FL imaging with inhomogeneous illumination (top) and NIR-II CL imaging with homogeneous illumination (bottom). Scale bar, 5 mm. (k) Corresponding intensity profiles along the capillary in (j).

maximum fluorescence and CL emission peak of the NIR-II CLS both blue-shift to 935 nm upon 540 nm excitation or by adding  $H_2O_2$ , respectively, which may be due to the self-aggregation of D-A-D dyes in the micelles (Figure 2e and Figure S2b). This result clearly indicated the successful occurrence of the effective DOD-to-BTD540 CRET and BTD540-to-BBTD700 FRET processes. Moreover, no obvious size alteration of NIR-II CLS was observed after storage in water for 10 days (Figure S5), indicating the excellent stability of NIR-II CLS. Thanks to the D-A-D structure and F127 shells, the as-prepared BTD540-BBTD700 micelle (without CPPO) showed tolerant antioxidant stability in the presence of  $H_2O_2$ , with more than 65% fluorescence intensity remained after 30 min (Figure 2f and Figure S6). To evaluate the advantage of CL in the NIR-II region, we compared the  $1/e$  tissue penetration depth<sup>[17]</sup> in two detection windows (600-800 nm and  $> 850$  nm, separated by corresponding optical filters) using chicken ham as mimic tissue. As shown in Figure 2g and 2h, the visibility of the CL signals deteriorated as the tissue depth increased from 0 to 8 mm for all the two detection windows. The deeper penetration depth ( $\sim 8$  mm) was observed in NIR-II region than

## COMMUNICATION

that in visible region ( $\sim 1 \text{ mm}$ ), suggesting that NIR-II region is the optimal window for deep tissue imaging. It is worth noting that the penetration depth in our system is still shallower than that of other excitation-free luminescence<sup>[18]</sup>, which may be caused by the relatively small molar extinction coefficient of the D-A-D structure dye molecule itself ( $\epsilon \approx 10^3\text{-}10^4 \text{ M}^{-1} \text{ cm}^{-1}$ ,  $\lambda_{\text{abs}} < 900 \text{ nm}$ )<sup>[19]</sup>.

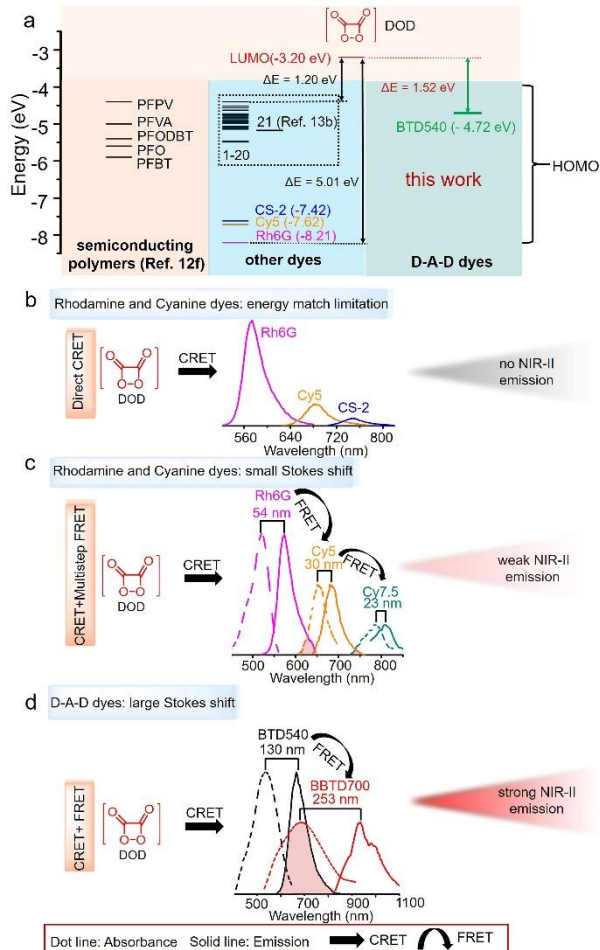


**Figure 3.** (a) The energy levels of most commonly adopted CRET acceptors and the active DOD intermediate. It should be noted that the energy gap between the HOMO level of BTD540 and the LUMO level of DOD intermediate is 1.52 eV, within the reasonable energy gap of the commonly CRET acceptors. The CL schemes of the direct CRET in (b) Rhodamine and Cyanine dyes, (c) CRET+Multistep FRET in Rhodamine and Cyanine dyes, (d) CRET+FRET processes in D-A-D dyes.

Due to the elimination of the external excitation light, CL would not suffer from the distorted signals in wide-field imaging as commonly occurred in FL imaging. To verify this, we studied the intensity distribution of a NIR-II CLS contained capillary in both CL (without excitation) and FL imaging modes (excited by 808 nm laser). As shown in Figure 2i, the laser beam followed a Gaussian point spread function (PSF) and the intensity distribution within the illumination site decreased from the center to the periphery with the maximum localized at the center. In NIR-II CL imaging, the uniform intensity was observed along the capillary tube (Figure 2j, bottom). However, we observed an incongruous intensity distribution along the capillary tube due to the

inhomogeneous illumination of the excitation light (Figure 2j, top) in NIR-II FL imaging. Even near the far end of the capillary tube, the NIR-II FL signal was attenuated to almost zero (Figure 2k). These results demonstrated that NIR-II CL without external light can be the better alternative for *in vivo* imaging.

It's worth noting that the appropriate dye type with efficient match of energy levels and large Stokes shift for the two energy transfer processes (CRET and FRET) are critical to realize efficient CL emission in NIR-II region (Figure 3). To realize efficient CRET, a proper energy gap between the LUMO level of DOD intermediate and the HOMO level of the acceptors is necessary. We summarize most commonly used CRET acceptors (Figure S7–S9), including semiconducting polymers and organic dyes<sup>[12f,13]</sup>, and calculated the energy gaps by performing density functional theory (DFT) (Figure 3a). A reasonable energy gap range between 1.20 eV and 5.01 eV is concluded out with the feasible CRET. In this work, the energy gap between the HOMO level of BTD540 and the LUMO level of DOD intermediate is 1.52 eV, which is within the above reasonable range, suggesting BTD540 is a proper CRET acceptor. On one hand, due to the energy match limitations, direct CRET process is unable to realize long wavelength CL in NIR-II region (Figure 3b). For example, we adopted three typical dyes (Rh6G, Cy5 or CS-2) with gradually prolonged absorption wavelengths. When encapsulated into the micelles separately with CPPO, the CL intensities of them decreased rapidly due to the gradually lowered CRET efficiencies (Figure S10). On the other hand, introducing FRET processes after CRET may extend the emission wavelength of CL to NIR-II region. However, the efficient energy transfer between the acceptor and donor is the key point to guarantee the strong CL emission. Taking the CPPO-Rh6G-Cy5-Cy7.5 micelle as an example (Figure 3c), although CL signal at 810 nm was detected by the multi-step FRET with small Stokes shift, it was very weak due to the accumulated energy loss in multiple energy transfer process (Figure S11). By contrast, the specially designed BTD540/BBTD700 as one-step FRET couple with excellent energy match as well as large Stokes shifts can guarantee the efficient energy transfer and the previously unreachable remarkable NIR-II CL (Figure 3d).

Next, we investigated the effects of  $\text{H}_2\text{O}_2$  concentration, temperature and reaction time on the efficiency of NIR-II CL. With increasing of  $\text{H}_2\text{O}_2$  concentration (3.5–13 mM) and temperature (15–45°C), the NIR-II CL signals were both increased gradually (Figure 4a–4h). At 15°C and 25°C, a sustained increase of CL intensity were observed with increasing  $\text{H}_2\text{O}_2$  concentration and time (Figure 4a and 4b, 4e and 4f). Further elevating the temperature to 37°C made CL signals continue to increase, with the strongest CL signal presented after 20 min upon the addition of  $\text{H}_2\text{O}_2$  (13 mM) (Figure 4g and 4j), and the corresponding intensity was 4.2-fold higher than that at 25°C (Figure 4i). The half-life of NIR-II CL was found to be 146 min, 136 min, 40 min and 40 min at 15°C, 25°C, 37°C and 45°C, respectively (Figure S12). When the temperature is increased up to 45°C, the CL signals were further increased 2.0 fold compared to that at 37°C and the maximum value was detected at 15 min (Figure 4d, 4h and 4i), which should be attributed to the promoted chemical reaction rate between CPPO and  $\text{H}_2\text{O}_2$ , which shortened reaction time with the temperature increasing. After reaching the emission peaks, the signal gradually decreased due to the decreasing

## COMMUNICATION

concentration of CPPO and  $\text{H}_2\text{O}_2$  with the progress of reaction. Therefore, the following *in vivo* CL imaging were conducted at physical temperature ( $37^\circ\text{C}$ ) within 60 min. In addition, NIR-II CLS exhibited excellent linear relationship to  $\text{H}_2\text{O}_2$  concentration and the CL limit of detection (LOD) was determined to be  $17.4 \mu\text{M}$  (Figure S13). Moreover, no CL signals were observed when  $\text{H}_2\text{O}_2$  was displaced by other reactive oxygen species ( $\text{ClO}^-$ ,  $\text{O}_2^-$ ,  $\text{ONOO}^-$  and  $\text{HO}^\bullet$ ) at  $37^\circ\text{C}$ , even prolonging the reaction time (Figure S14), indicating the good selectivity of NIR-II CLS to  $\text{H}_2\text{O}_2$  (Figure 4k).

The reliable *in vitro* spectral properties and selectivity test for  $\text{H}_2\text{O}_2$  with NIR-II CLS encouraged us to further explore its potential for *in vivo* NIR-II CL imaging. First, the potential cytotoxicity of NIR-II CLS was evaluated in human umbilical vein endothelial cells (HUVEC), which showed over 87% viability after incubation with  $6.2 \text{ mg mL}^{-1}$  nanosensor for 24 h, indicating the low cytotoxicity of NIR-II CLS (Figure S15). We next carried out lymphatic and arthritis inflammation imaging models (Figure 5a) for NIR-II CL bioimaging using the home-built small animal system

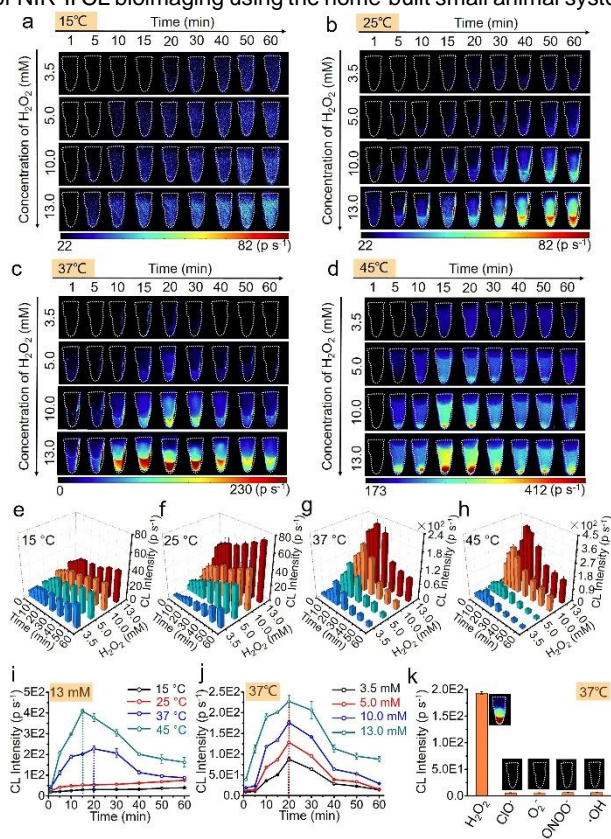


**Figure 4.** The CL imaging of NIR-II CLS ( $8.2 \text{ mg mL}^{-1}$ ) upon addition of different concentration of  $\text{H}_2\text{O}_2$  at (a)  $15^\circ\text{C}$ , (b)  $25^\circ\text{C}$ , (c)  $37^\circ\text{C}$  and (d)  $45^\circ\text{C}$ . (e-h) Corresponding NIR-II CL signals upon addition of different concentration  $\text{H}_2\text{O}_2$  in (a-d), respectively. (i) Time-dependent NIR-II CL signal intensities upon addition of  $\text{H}_2\text{O}_2$  ( $13 \text{ mM}$ ) at  $15\text{--}45^\circ\text{C}$ . (j) Time-dependent CL signal intensities upon addition of different concentration  $\text{H}_2\text{O}_2$  at  $37^\circ\text{C}$ . (k) NIR-II CL signal intensities of NIR-II CLS ( $8.2 \text{ mg mL}^{-1}$ ) upon addition of various ROS ( $13 \text{ mM}$ ) at  $37^\circ\text{C}$ . Insert: Corresponding NIR-II CL imaging upon addition of various ROS.

(Figure S16). To show the advantages of NIR-II CL imaging in our designed system based on the D-A-D dyes, we took NIR-II FL

imaging in the same mouse by adopted micelle containing only BDTD700 as the reference.

The lymphatic inflammation model of mice was established by intradermal injection into the rear paw of  $34 \text{ mM}$  ( $75 \mu\text{L}$ ) hydrogen peroxide. Then, BDTD700 micelle was injected intradermally at the rear paw of mouse, and NIR-II FL signal was detected in the lymph node region with the highest SNR of only 1.40 after 40 min post-injection under 808 nm laser excitation (Figure 5b and S17). In comparison, the NIR-II CL signal was quickly observed in the lymph node region at 1 min after intradermal injection of NIR-II CLS at the rear paw of mouse, and then the signal decreased due to the fast flow of  $\text{H}_2\text{O}_2$  in mouse (Figure S18). Even though, 3.4-fold enhancement of SNR was obtained in the CL imaging (4.74) compared to that of NIR-II FL (1.40) due to the ultralow tissue autofluorescence background in the absence of excitation light (Figure 5b). In addition to the elimination of background noise, the absence of external light may also avoid the risk of overheating when performing CL imaging. In comparison, a 808 nm laser, which can excite NIR-II CLS used in conventional FL imaging, indeed increased the skin temperature of a nude mouse by  $\sim 5^\circ\text{C}$  within 60 min and it continued to rise (Figure 5c). This might be destructive to the living body.

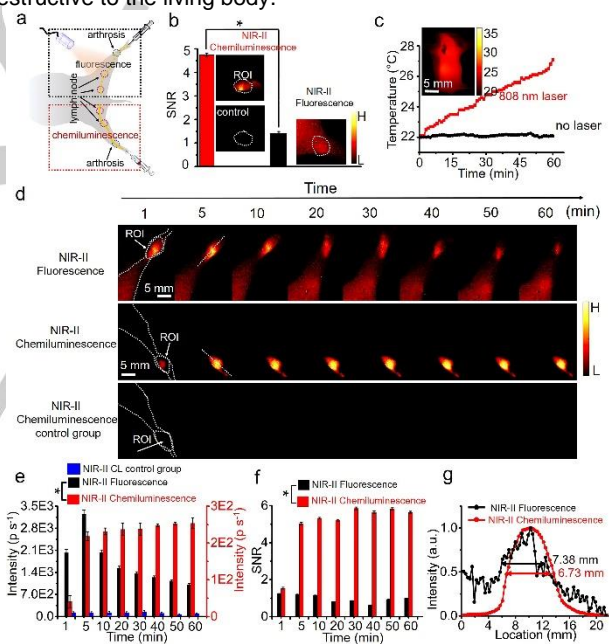


**Figure 5.** (a) Schematic illustration of executing CL and FL imaging carrying on mice lymph node and arthritis. For FL imaging, 808 nm excitation light with 800 ms exposure time ( $P = 32 \text{ mW cm}^{-2}$ ) was adopted. (b) The comparison of SNR between the NIR-II CL imaging (1 min post-injection of  $0.98 \text{ mg}$  NIR-II CLS) and the NIR-II FL imaging (40 min post-injection of  $1.2 \text{ mg}$  BDTD700 micelle) of lymphatic inflammation,  $*P < 0.05$ . Insert: corresponding images of lymphatic node ( $n = 3$ ). (c) Temperature variation curves of nude mouse skin recorded with and without laser irradiation ( $808 \text{ nm}$ ,  $94 \text{ mW cm}^{-2}$ ). Insert: Skin temperature of nude mouse irradiated at 60 min. Scale bar, 5 mm,  $n = 3$ . (d) *In vivo* NIR-II FL imaging (top panel) of BDTD700 micelle ( $1.2 \text{ mg}$ ) and NIR-II CL imaging (middle panel) of arthritis inflammation with NIR-II CLS ( $0.92 \text{ mg}$ ) at different post-injection time, respectively. Control experiments with healthy mice for NIR-II CL imaging of arthritis with NIR-II CLS ( $0.92 \text{ mg}$ ) were also carried out for comparison (bottom panel). The corresponding NIR-II CL/FL signals intensity (e) and SNRs (f) in (d) as a function of post-injection time,  $*P < 0.05$ . (g) Intensity profiles along the arthritis position of a mouse (the white line in 5d). Scale bar, 5 mm. Bars represent mean  $\pm$  s.d. ( $n = 3$ ). (850 nm long-pass filter).

## COMMUNICATION

The arthritis inflammation model of mice was established by intra-articular injection of 33 mM (75  $\mu$ L) hydrogen peroxide, then NIR-II CLS were used by sequentially intra-articular injection into a mouse. With the progress of reaction with H<sub>2</sub>O<sub>2</sub>, the CL signals and SNRs in the arthritis area were increased over time (Figure 5d-f). The maximum SNR of 5.85 in the arthritis area was observed at 30 min. We also acquired the NIR-II FL signals with BBTD700 micelle (Figure 5d). The FL signal was gradually increased to a maximum at 5 min post-injection and dropped 44% at 60 min (Figure 5e). During this whole period, the maximum FL SNR of 1.24 in the arthritis area was obtained at 5 min, which was still 4.5-fold lower than that with CL imaging (Figure 5f). Besides, the smaller full width at half maxima (FWHM = 6.73 nm) of the arthritis position tracing in CL imaging over NIR-II FL imaging (FWHM = 7.38 nm) also showed superior accuracy (Figure 5g). For comparison, we also carried out control experiment on the lymphatic and arthritis imaging with healthy mice. No CL signals were observed in the above two regions due to the lack of H<sub>2</sub>O<sub>2</sub>. Based on the above results, NIR-II CLS can achieve higher SNR for *in vivo* inflammation imaging.

In summary, we have developed a NIR-II CL sensor for overcoming the drawbacks of short-wavelength CL emission and lower penetration depth through engineering the cascade CRET and FRET processes. The as-prepared biocompatible NIR-II CLS have deeper penetration depth and higher SNR for *in vivo* CL inflammation imaging. To reduce the energy loss during multi-step energy transfer, we rationally designed the dyes with excellent energy match and the large Stokes shift characteristics to efficiently transfer the chemical energy, which made a better foundation for the development of *in vivo* CL NIR-II imaging. It provides a promising perspective and strategy for constructing probes with extended emission wavelength in classical CL for higher contrast imaging. Meanwhile, it also offers the possibility of sensing various analytes by changing the chemiluminescent substrate in the future. Although the sensitivity and brightness of the current NIR-II CLS shown here is still not ideal, the present results indicated that the NIR-II CLS is promising for NIR-II CL *in vivo* imaging with higher SNR compared to the NIR-II fluorescence signals in the same system. Besides, the NIR-II CLS may be further improved by rationally designing probes with higher quantum yield (for example, the introduction of substituted thiophene and shielding units<sup>[19]</sup>), larger molar extinction coefficient, and better oxidation resistance. Given CL imaging immune to background interference and light damage from the external excitation light, it could motivate more pre-clinical and clinical translation applications.

## Acknowledgements

The work was supported by the National Key R&D Program of China (2017YFA0207303), National Natural Science Foundation of China (NSFC, 21725502, 51961145403), and Key Basic Research Program of Science and Technology Commission of Shanghai Municipality (17JC1400100).

**Keywords:** NIR-II imaging • chemiluminescence imaging • bioimaging • inflammation tracing •

- [1] a) M. Bates, B. Huang, G. T. Dempsey, X. Zhuang, *Science* **2007**, *317*, 1749-1753; b) T.-L. Liu, S. Upadhyayula, D. E. Milkie, V. Singh, K. Wang, I. A. Swinburne, K. R. Mosaliganti, Z. M. Collins, T. W. Hiscock, J. Shea, A. Q. Kohrman, T. N. Medwig, D. Dambournet, R. Forster, B. Cunniff, Y. Ruan, H. Yashiro, S. Scholpp, E. M. Meyerowitz, D. Hockemeyer, D. G. Drubin, B. L. Martin, D. Q. Matus, M. Koyama, S. G. Megason, T. Kirchhausen, E. Betzig, *Science* **2018**, *360*, eaaq1392; c) R. Gao, S. M. Asano, S. Upadhyayula, I. Pisarev, D. E. Milkie, T.-L. Liu, V. Singh, A. Graves, G. H. Huynh, Y. Zhao, J. Bogovic, J. Colonell, C. M. Ott, C. Zugates, S. Tappan, A. Rodriguez, K. R. Mosaliganti, S.-H. Sheu, H. A. Pasolli, S. Pang, C. S. Xu, S. G. Megason, H. Hess, J. Lippincott-Schwartz, A. Hantman, G. M. Rubin, T. Kirchhausen, S. Saalfeld, Y. Aso, E. S. Boyden, E. Betzig, *Science* **2019**, *363*, eaau8302.
- [2] a) G. Hong, A. L. Antaris, H. Dai, *Nat. Biomed. Eng.* **2017**, *1*, 0010; b) J. Huang, J. Li, Y. Lyu, Q. Miao, K. Pu, *Nat. Mater.* **2019**, *18*, 1133-1143; c) S. Wang, Y. Fan, D. Li, C. Sun, Z. Lei, L. Lu, T. Wang, F. Zhang, *Nat. Commun.* **2019**, *10*, 1058; d) A. L. Antaris, H. Chen, K. Cheng, Y. Sun, G. Hong, C. Qu, S. Diao, Z. Deng, X. Hu, B. Zhang, X. Zhang, O. K. Yaghi, Z. R. Alamparambil, X. Hong, Z. Cheng, H. Dai, *Nat. Mater.* **2016**, *15*, 235-242; e) Q. G. Zang, J. Y. Yu, W. B. Yu, J. Qian, R. R. Hu, B. Z. Tang, *Chem. Sci.* **2018**, *9*, 5165-5171; f) C. Sun, B. Li, M. Zhao, S. Wang, Z. Lei, L. Lu, H. Zhang, L. Feng, C. Dou, D. Yin, H. Xu, Y. Cheng, F. Zhang, *J. Am. Chem. Soc.* **2019**, *141*, 19221-19225; g) Y. Li, X. Li, Z. Xue, M. Jiang, S. Zeng, J. Hao, *Biomaterials* **2018**, *169*, 35-44; h) Y. Yang, P. Wang, L. Lu, Y. Fan, C. Sun, L. Fan, C. Xu, A. M. El-Toni, M. Alhoshan, F. Zhang, *Anal. Chem.* **2018**, *90*, 7946-7952; i) S. He, J. Song, J. Qu, Z. Chen, *Chem. Soc. Rev.* **2018**, *47*, 4258-4278; j) Kenry, Y. Duan, B. Liu, *Adv. Mater.* **2018**, *30*, 1802394; k) Y. Miao, C. Gu, Y. Zhu, B. Yu, Y. Shen, H. Cong, *ChemBioChem.* **2018**, *19*, 2522-2541; l) J. A. Carra, M. Aellena, D. Franke, P. T. C. So, O. T. Brunsa, M. G. Bawendia, *Proc. Natl. Acad. Sci. U. S. A.* **2018**, *115*, 9080-9085; m) F. Ding, C. Li, Y. Xu, J. Li, H. Li, G. Yang, Y. Sun, *Adv. Healthc. Mater.* **2018**, *7*, 1800973; n) A. M. Smith, M. C. Mancini, S. Nie, **2009**, *4*, 710-711; o) X. Zeng, Y. Xiao, J. Lin, S. Li, H. Zhou, J. Nong, G. Xu, H. Wang, F. Xu, J. Wu, Z. Deng, X. Hong, *Adv. Healthc. Mater.* **2018**, *7*, 1800589; p) Y. Sun, X. Zeng, Y. Xiao, C. Liu, H. Zhu, H. Zhou, Z. Chen, F. Xu, J. Wang, M. Zhu, J. Wu, M. Tian, H. Zhang, Z. Deng, Z. Chen, X. Hong, *Chem. Sci.* **2018**, *9*, 2092-2097; q) X. Gao, Y. Cui, R. M. Levenson, L. W. K. Chung, S. Nie, *Nat. Biotechnol.* **2004**, *22*, 969-976; r) S. L. Jacques, *Phy. Med. Biol.* **2013**, *58*, R37-R61; s) H. Maeda, T. Kowada, J. Kikuta, M. Furuya, M. Shirazaki, S. Mizukami, M. Ishii, K. Kikuchi, *Nat. Chem. Biol.* **2016**, *12*, 579-585; t) W. Zheng, P. Huang, Z. Gong, D. Tu, J. Xu, Q. Zou, R. Li, W. You, J.-C. G. Bünzli, X. Chen, *Nat. Commun.* **2018**, *9*, 3462; u) E. Y. Zhou, H. J. Knox, C. J. Reinhardt, G. Partipilo, M. Nilges, J. Chan, *J. Am. Chem. Soc.* **2018**, *140*, 11686-11697; v) C. J. Reinhardt, R. Xu, J. Chan, *Chem. Sci.* **2020**, *11*, 1587-1592; w) Y. Sang, F. Cao, W. Li, L. Zhang, Y. You, Q. Deng, K. Dong, J. Ren, X. Qu, *J. Am. Chem. Soc.* **2020**, *142*, 5177-5183. x) J. Huang, K. Pu, *Angew. Chem. Int. Ed.* **2020**, *59*, 2-17.
- [3] a) B. Del Rosal, D. H. Ortgies, N. Fernandez, F. Sanz-Rodriguez, D. Jaque, E. M. Rodriguez, *Adv. Mater.* **2016**, *28*, 10188-10193; b) M. Y. Berezin, S. Achilefu, *Chem. Rev.* **2010**, *110*, 2641-2684.
- [4] a) S. Diao, G. Hong, A. L. Antaris, J. L. Blackburn, K. Cheng, Z. Cheng, H. Dai, *Nano Res.* **2015**, *8*, 3027-3034; b) J. Ruff, S. Hüwel, M. J. Kogan, U. Simon, H. J. Galla, *Nanomedicine* **2017**, *13*, 1645-1652.
- [5] L. Hu, G. Xu, *Chem. Soc. Rev.* **2010**, *39*, 3275-3304.
- [6] E. A. Chandross, *Tetrahedron Lett.* **1963**, *4*, 761-765.
- [7] a) A. M. Garcia-Campana, W. R. G. Baeyens, *Chemiluminescence in Analytical Chemistry*, Marcel Dekker, NY, USA, **2001**; b) P. A. Wingert, H. Mizukami, A. E. Ostafin, *Nanotechnology* **2007**, *18*, 295707; c) X. Huang, L. Li, H. Qian, C. Dong, J. Ren, *Angew. Chem. Int. Ed.* **2006**, *45*, 5140-5143; d) H. Wang, Y. Li, J. Wang, Q. Xu, X. Li, Y. Zhao, *Anal. Chim. Acta* **2008**, *610*, 68-73.
- [8] a) G. B. Schuster, *Accounts Chem. Res.* **1979**, *12*, 366-373; b) T. Wilson, *Photochem. Photobiology.* **1995**, *62*, 601-606; c) J.-Y. Koo, G. B. Schuster, *J. Am. Chem. Soc.* **1977**, *99*, 6107-6109; d) J. A. Koo, S. P. Schmidt, G. B. Schuster, *Proc. Natl. Acad. Sci. U. S. A.* **1978**, *75*, 30-33; e) J.-Y. Koo, G. B. Schuster, *J. Am. Chem. Soc.* **1978**, *100*, 4496-4503.

## COMMUNICATION

- [9] D. J. Naczynski, M. C. Tan, M. Zevon, B. Wall, J. Kohl, A. Kulesa, S. Chen, C. M. Roth, R. E. Riman, P. V. Moghe, *Nat. Commun.* **2013**, *4*, 2199.
- [10] D. Lee, S. Khaja, J. C. Velasquez-Castano, M. Dasari, C. Sun, J. Petros, W. R. Taylor, N. Murthy, *Nat. Mater.* **2007**, *6*, 765-769.
- [11] L. Zhang, N. He, C. Lu, *Anal. Chem.* **2015**, *87*, 1351-1357.
- [12] a) C. K. Lim, Y. D. Lee, J. Na, J. M. Oh, S. Her, K. Kim, K. Choi, S. Kim, I. C. Kwon, *Adv. Funct. Mater.* **2010**, *20*, 2644-2648; b) Y. H. Seo, A. Singh, H.-J. Cho, Y. Kim, J. Heo, C.-K. Lim, S. Y. Park, W.-D. Jang, S. Kim, *Biomaterials* **2016**, *84*, 111-118; c) D. Lee, S. Khaja, J. C. Velasquez-Castano, M. Dasari, C. Sun, J. Petros, W. R. Taylor, N. Murthy, *Nat. Mater.* **2007**, *6*, 765-769; d) Y. D. Lee, C. K. Lim, A. Singh, J. Koh, J. Kim, I. C. Kwon, S. Kim, *ACS Nano* **2012**, *6*, 6759-6766; e) A. J. Shuhendler, K. Pu, L. Cui, J. P. Uetrecht, J. Rao, *Nat. Biotechnol.* **2014**, *32*, 373-380; f) X. Zhen, C. Zhang, C. Xie, Q. Miao, K. L. Lim, K. Pu, *ACS Nano* **2016**, *10*, 6400-6409; g) A. Singh, H.-J. Cho, S. Lee, J. Koh, S. Kim, *Macromol. Res.* **2014**, *22*, 1136-1139; h) S. Cho, O. Hwang, I. Lee, G. Lee, D. Yoo, G. Khang, P. M. Kang, D. Lee, *Adv. Funct. Mater.* **2012**, *22*, 4038-4043.
- [13] a) S. Kim, *ACS Nano* **2015**, *9*, 9906-9911; b) D. Mao, W. Wu, S. Ji, C. Chen, F. Hu, D. Kong, D. Ding, B. Liu, *Chem* **2017**, *3*, 991-1007.
- [14] a) P. Cheng, Q. Miao, J. Li, J. Huang, C. Xie, K. Pu, *J. Am. Chem. Soc.* **2019**, *141*, 10581-10584; b) J. Huang, Y. Lyu, J. Li, P. Chen, Y. Jiang, K. Pu, *Angew. Chem. Int. Ed.* **2019**, *58*, 17796-17804; c) N. Hananya, D. Shabat, *Angew. Chem. Int. Ed.* **2017**, *56*, 16454-16463; d) S. Gnaim, O. Green, D. Shabat, *Chem. Commun.* **2018**, *54*, 2073-2085; e) S. Gnaim, A. Scomparin, A. Eldar-Boock, C. R. Bauer, R. Satchi-Fainaro, D. Shabat, *Chem. Sci.* **2019**, *10*, 2945-2955; f) D. Cui, J. Li, X. Zhao, K. Pu, R. Zhang, *Adv. Mater.* **2020**, *32*, 1906314.
- [15] a) M. Ehsani, M. J. Chaichi, S. N. Hosseini, *Sensors Actuat. B-Chem.* **2017**, *247*, 319-328; b) H. Arakawa, K. Tsuruoka, K. Ohno, N. Tajima, H. Nagano, *Luminescence* **2014**, *29*, 374-377; c) C. Shim, R. Chong, J. H. Lee, *Talanta* **2017**, *171*, 229-235.
- [16] A. T. R. Williams, S. A. Winfield, J. N. Miller, *The Analyst* **1983**, 108.
- [17] a) Q. Zhao, C. Dai, S. Fan, J. Lv, L. Nie, *Sci Rep.* **2016**, *6*, 34954; b) Q. Zhao, H. Wei, Y. He, Q. Ren, C. Zhou, *J. Biophotonics* **2014**, *7*, 938-947.
- [18] a) Y. Jiang, J. Huang, X. Zhen, Z. Zeng, J. Li, C. Xie, Q. Miao, J. Chen, P. Chen, K. Pu, *Nat. Commun.* **2019**, *10*, 2064; b) Q. Miao, C. Xie, X. Zhen, Y. Lyu, H. Duan, X. Liu, J. V. Jokerst, K. Pu, *Nat. Biotechnol.* **2017**, *35*, 1102.
- [19] Q. Yang, Z. Hu, S. Zhu, R. Ma, H. Ma, Z. Ma, H. Wan, T. Zhu, Z. Jiang, W. Liu, L. Jiao, H. Sun, Y. Liang, H. Dai, *J. Am. Chem. Soc.* **2018**, *140*, 1715-1724.

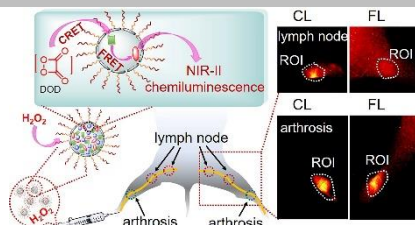
## COMMUNICATION

Entry for the Table of Contents (Please choose one layout)

Layout 1:

## COMMUNICATION

Novel NIR-II chemiluminescence sensor was prepared by cascade CRET and one-step FRET for *in vivo* high contrast inflammation imaging.



Yanling Yang, Shangfeng Wang,  
Lingfei Lu, Qisong Zhang, Peng Yu,  
Yong Fan\*, Fan Zhang\*

Page No. – Page No.

**NIR-II Chemiluminescence  
Molecular Sensors for In-Vivo High  
Contrast Inflammation Imaging**